

Machine Learning-Driven High-Precision Model for α -Decay Energy and Half-Life Prediction of superheavy nuclei

Qingning Yuan, Panpan Qi, Xuanpen Xiao, Xue Wang, Juan He, Guimei Long, Zhengwei Duan, Yangyan Dai, Runchao Yan and Gongming Yu^{1a} Haitao Yang^{2b}

^aCollege of Physics and Technology, Kunming University, Kunming 650214, China.

^bCollege of Science, Zhaotong University, Zhaotong 657000, China.

E-mail: ygmanan@kmu.edu.cn, yanghaitao205@163.com

ABSTRACT: We develop a physics-informed machine-learning framework for predicting α -decay energies and half-lives across a broad range of nuclei. The approach is built on an eXtreme Gradient Boosting (XGBoost) regression model and integrates physically motivated nuclear descriptors. For half-life prediction, key structure-related features—such as magic-number proximity, minimum orbital angular-momentum transfer, isospin asymmetry, and quadrupole deformation—are incorporated to reflect the dominant mechanisms governing α decay within a data-driven model. On independent test nuclei, the proposed model achieves high predictive accuracy without evident overfitting. Benchmark comparisons with widely used empirical formulations, including the Royer and Universal Decay Law (UDL) expressions, show that the XGBoost model yields lower overall prediction errors while preserving the established systematics of α -decay observables. SHapley Additive exPlanations (SHAP) analysis further demonstrates that the leading contributions of decay-energy information, centrifugal hindrance, and shell-related effects follow physically consistent trends, supporting the interpretability of the learned mapping. These results indicate that gradient-boosting models equipped with physics-guided features can provide accurate, robust, and interpretable tools for α -decay systematics and for extrapolating half-lives in regions where measurements are limited.

¹Corresponding author

²Corresponding author

Contents

1	Introduction	1
2	General Formalism	4
2.1	The Mathematical Fundamentals of eXtreme Gradient Boosting	4
2.2	Data input and feature engineering construction	6
2.2.1	Decay Energy Prediction	7
2.2.2	Half-life Prediction	7
2.3	Empirical Formulas (Royer and Universal Decay Law)	9
2.3.1	Royer Formula	9
2.3.2	Universal Decay Law Formula	10
3	Results and Discussion	11
3.1	Decay Energy Prediction Performance	11
3.2	Half-Life Prediction Performance	12
4	Summary and Conclusion	16
5	Acknowledgements	17

1 Introduction

The study of α decay dates back to the early stages of research on radioactivity. In 1899, Rutherford and collaborators, while investigating uranium-series emissions, first distinguished a radiation component characterized by low penetration but strong ionization, and designated it as the α ray. Subsequent systematic experiments conducted in 1909 further confirmed that α particles are doubly charged helium nuclei. This key discovery not only clarified the microscopic nature of radioactive emissions but also established an essential experimental foundation for the development of nuclear-structure models and for understanding nuclear stability. As experimental data continued to accumulate, the regularities underlying α decay gradually emerged, providing a solid foundation for subsequent systematic investigations of α -decay behavior and for the later development of the quantum-tunneling description of nuclear decay [1–3]. Consequently, α decay soon became not only an essential topic in early nuclear physics but also a key phenomenon for revealing the structure and stability of atomic nuclei. Building on the accumulating experimental evidence, Geiger and Nuttall (1911) identified a clear correlation between the α -decay half-life and the decay energy. This analysis led to the formulation of the Geiger-Nuttall law, which expresses a logarithmic linear dependence of the half-life on the released decay energy.

The emergence of this empirical relation provided a crucial foundation for subsequent phenomenological descriptions of radioactive decay and significantly advanced the quantitative understanding of nuclear disintegration dynamics [4–6].

Following the empirical establishment of the Geiger–Nuttall law, the subsequent development of quantum mechanics provided a deeper physical interpretation of its underlying regularities. In 1928, Gamow introduced the pioneering quantum-tunneling model, which for the first time explained the emission of α particles as a consequence of their ability to penetrate the Coulomb barrier. This framework naturally reproduced the characteristic exponential dependence of the half-life on the decay energy and offered a rigorous theoretical foundation for the Geiger–Nuttall relation, marking a transition toward a quantitative and microscopic understanding of α decay. Building upon Gamow’s theoretical insight, numerous empirical or semi-empirical formulas were later developed to predict the logarithm of α -decay half-lives, among which the Royer formula and the Universal Decay Law (UDL) have been widely adopted in nuclear-structure and decay studies [7–10]. Continuous improvements driven by theoretical advances and the expansion of experimental databases have enhanced the predictive accuracy of these phenomenological models across broad regions of the nuclear chart. Nevertheless, their fixed functional forms limit the degree to which shell effects, deformation, and angular-momentum hindrance can be fully incorporated, motivating the exploration of approaches that integrate richer physical constraints or data-driven methodologies. Although these empirical formulations incorporate nucleon-parity effects and employ distinct parameter sets for different categories of nuclei, they often exhibit pronounced systematic deviations in low-energy regions or for nuclei far from the valley of stability. This limitation primarily arises from the fact that their fitted parameters are derived from experimental datasets densely concentrated near the stability line and at relatively high Q_α values. In contrast, nuclei in low- Q_α or more exotic regions frequently suffer from substantial experimental uncertainties, thereby reducing both the reliability and the generalizability of these models. Moreover, lower Q_α values correspond to sharply reduced barrier-penetration probabilities, which display exponential sensitivity to small variations in Q_α . As a result, even minor deviations in decay energy may lead to orders-of-magnitude discrepancies in half-life predictions. In addition, the simplified treatments of potential-barrier structure and tunneling dynamics adopted in these empirical approaches, though adequate near the fitted domains, tend to amplify errors as the decay energy decreases, further intensifying their inherent systematic deviations [11–13].

Recent advances in computational technologies have substantially enhanced data processing and analysis capabilities, thereby accelerating the integration of machine-learning techniques across numerous scientific domains. In physics—where the objective is to uncover the fundamental properties of matter and the governing laws of natural phenomena—machine learning has increasingly emerged as a powerful tool for addressing complex problems. Traditional approaches that rely on mathematical modeling, experimental observation, and numerical simulation often face significant challenges when dealing with high-dimensional phase spaces, multiscale systems, or strongly correlated phenomena. Under such circumstances, computational costs become prohibitive and accurate theoretical descriptions may be lacking, ultimately constraining both predictive accuracy and

model generalizability [14–18]. To address the limitations of traditional empirical formulas, machine-learning (ML) techniques have increasingly been adopted for modeling nuclear decay properties, particularly α decay. A variety of ML algorithms—including artificial neural networks (ANN), support vector machines (SVM), Gaussian processes (GP), and gradient-boosting methods such as XGBoost—have demonstrated strong predictive capabilities for α -decay energies and half-lives. These approaches are capable of capturing complex non-linear dependencies between nuclear-structure features and decay observables, and in many cases surpass the performance of traditional empirical formulas, especially for nuclei in low- Q_α regions or far from the valley of stability [19–23].

Despite recent progress in nuclear-decay modeling, most existing machine-learning approaches still face challenges related to limited precision control and susceptibility to overfitting or underfitting. Furthermore, systematic comparisons with classical empirical formulas across different energy regimes remain insufficient, hindering a comprehensive assessment of model performance. The interpretability of many machine-learning models also requires further improvement, as their internal decision mechanisms often lack clear connections to underlying nuclear-structure physics.

Furthermore, high-quality experimental data for exotic nuclei—particularly those far from the valley of stability or in low decay-energy regions—remain inherently scarce. This scarcity constrains not only the refinement of empirical models but also the development of robust and generalizable data-driven approaches. As a result, constructing models that can deliver accurate and physically consistent predictions under limited-data conditions has become an essential objective in contemporary nuclear-decay research.

To address these challenges, this study introduces an integrated and interpretable machine-learning framework for the simultaneous prediction of α -decay energies and half-lives. The model is built upon the XGBoost regression algorithm and incorporates a set of physically motivated nuclear-structure features, including mass number, neutron–proton asymmetry, shell proximity quantified through magic-number distance, and the minimum angular-momentum transfer. Model performance is rigorously benchmarked against traditional empirical formulas, such as the Royer expression and the UDL, using both training and independent test sets. Furthermore, SHAP-based feature attribution is employed to elucidate the dominant physical mechanisms captured by the model, thereby enhancing interpretability and establishing clear connections between data-driven predictions and underlying α -decay physics.

This paper is organized as follows. Section 2 describes the XGBoost-based framework employed in this study, including feature construction, data preprocessing, and the overall training procedure. Section 3 presents a detailed analysis of the model’s performance in predicting α -decay energies and half-lives, together with comparisons against traditional empirical formulas and SHAP-based interpretations of the underlying physical trends. Finally, Section 4 summarizes the principal findings of this work.

2 General Formalism

This section outlines the systematic modeling workflow adopted in this study, including the fundamental principles of the XGBoost method, the training strategy incorporating an early-stopping mechanism, the feature-engineering procedure, the model parameter configuration and analysis, and the benchmarking methodology against traditional empirical formulas. The experimental dataset used in this work is compiled from Refs. [23–27] and undergoes appropriate preprocessing before being utilized for both machine-learning training and empirical-formula evaluation.

Alpha decay is a quantum tunneling process in which a preformed α particle escapes the parent nucleus by penetrating the nuclear potential barrier. Its half-life can be described within the framework of Gamow theory, which employs the Wentzel–Kramers–Brillouin (WKB) approximation to evaluate the tunneling probability. In the standard WKB treatment, the α particle is assumed to be preformed inside the parent nucleus and subsequently tunnels through an effective potential barrier composed of nuclear attraction, Coulomb repulsion, and a centrifugal term. The tunneling probability is predominantly determined by the Gamow factor derived from the WKB approximation [13, 28, 29].

$$P = \exp \left[-\frac{2}{\hbar} \int_{R_{\text{in}}}^{R_{\text{out}}} \sqrt{2\mu(V(r) - Q_\alpha)} dr \right], \quad (2.1)$$

where μ is the reduced mass, $V(r)$ denotes the effective potential energy, Q_α is the decay energy, and R_{in} and R_{out} are the classical turning points. This formulation explicitly highlights the central role of the decay energy Q_α in governing the tunneling probability, as variations in Q_α enter exponentially and therefore exert a dominant influence on the resulting half-life. Following Ref. [13], the α -decay half-life can be expressed as:

$$T_{1/2} = \frac{\ln 2}{\lambda} = \frac{\ln 2}{\nu S_c P}, \quad (2.2)$$

where λ denotes the decay constant, ν is the assault frequency, and P is the tunneling probability. As shown in Eqs. (2.1) and (2.2), even small variations in the input parameters can lead to changes of several orders of magnitude in the calculated half-life. This extreme sensitivity arises primarily from the exponential dependence of the penetration probability P on the decay energy Q_α . Consequently, any uncertainty in Q_α propagates exponentially and introduces substantial uncertainty into the predicted half-life [30, 31].

Moreover, because α -decay half-lives typically span several orders of magnitude, this broad dynamic range presents significant challenges for data modeling and regression analysis. To enhance numerical stability and reduce the influence of extreme values during training, the present study adopts the base-10 logarithm of the half-life, $\log_{10} T_{1/2}$, as the regression target [32, 33].

2.1 The Mathematical Fundamentals of eXtreme Gradient Boosting

In this work, the Extreme Gradient Boosting (XGBoost) algorithm is employed as the regression framework for learning the nonlinear mapping between nuclear-structure features

and decay observables. XGBoost constructs its predictor as an additive ensemble of regression trees, where the model output for a given sample \mathbf{x}_i is expressed as [34, 35]:

$$\hat{y}_i = \sum_{k=1}^K f_k(\mathbf{x}_i), \quad f_k \in \mathcal{F}, \quad (2.3)$$

with \mathcal{F} denoting the functional space of CART regression trees. Each tree f_k assigns a constant prediction to samples falling into the same leaf node, and can therefore be written as:

$$f(\mathbf{x}) = w_{q(\mathbf{x})}, \quad q: \mathbb{R}^m \rightarrow \{1, 2, \dots, L\}, \quad (2.4)$$

where L is the number of leaf nodes, $q(\mathbf{x})$ specifies the leaf index to which \mathbf{x} is mapped, and w_j is the weight associated with the j -th leaf. XGBoost employs a forward stagewise procedure, in which the model at iteration t is obtained by adding a new tree f_t to the previous ensemble, such that [36]

$$\hat{y}_i^{(t)} = \hat{y}_i^{(t-1)} + f_t(\mathbf{x}_i). \quad (2.5)$$

To suppress overfitting and enhance generalization, XGBoost minimizes a regularized objective function composed of a training loss and a structural penalty on the regression trees [37, 38]:

$$\mathcal{L}^{(t)} = \sum_i l(y_i, \hat{y}_i^{(t)}) + \sum_{k=1}^t \Omega(f_k). \quad (2.6)$$

In the present study the mean-squared-error loss is adopted,

$$l(y_i, \hat{y}_i) = \frac{1}{2}(y_i - \hat{y}_i)^2, \quad (2.7)$$

while the regularization term penalizes overly complex trees via

$$\Omega(f_t) = \gamma L_t + \frac{1}{2} \lambda \sum_{j=1}^{L_t} w_{tj}^2, \quad (2.8)$$

where L_t denotes the number of leaf nodes in tree f_t , γ controls the creation of new leaves, and λ regulates the magnitude of leaf weights. Since only f_t is newly introduced at iteration t , the loss contribution of this tree is isolated by expanding the objective using a second-order Taylor approximation around the previous prediction $\hat{y}_i^{(t-1)}$ [39, 40]:

$$l(y_i, \hat{y}_i^{(t-1)} + f_t(\mathbf{x}_i)) \approx l(y_i, \hat{y}_i^{(t-1)}) + g_i f_t(\mathbf{x}_i) + \frac{1}{2} h_i f_t^2(\mathbf{x}_i), \quad (2.9)$$

where

$$g_i = \left. \frac{\partial l}{\partial \hat{y}} \right|_{\hat{y}_i^{(t-1)}}, \quad h_i = \left. \frac{\partial^2 l}{\partial \hat{y}^2} \right|_{\hat{y}_i^{(t-1)}}, \quad (2.10)$$

and for the MSE loss employed here, $g_i = \hat{y}_i^{(t-1)} - y_i$ and $h_i = 1$. Substituting Eq. (2.9) into Eq. (2.6) and discarding constants yields the approximate objective for optimizing the new tree:

$$\tilde{\mathcal{L}}^{(t)} = \sum_i \left[g_i f_t(\mathbf{x}_i) + \frac{1}{2} h_i f_t^2(\mathbf{x}_i) \right] + \Omega(f_t). \quad (2.11)$$

Since $f_t(\mathbf{x}_i) = w_j$ for all samples belonging to leaf j , let $I_j = \{i \mid q(\mathbf{x}_i) = j\}$ denote the index set of samples falling into this leaf. Defining the aggregated first- and second-order gradients as

$$G_j = \sum_{i \in I_j} g_i, \quad H_j = \sum_{i \in I_j} h_i, \quad (2.12)$$

the objective Eq. (2.11) becomes

$$\tilde{\mathcal{L}}^{(t)} = \sum_{j=1}^{L_t} \left[G_j w_j + \frac{1}{2} (H_j + \lambda) w_j^2 \right] + \gamma L_t. \quad (2.13)$$

Minimizing this expression with respect to each leaf weight yields the optimal solution [41]:

$$w_j^* = -\frac{G_j}{H_j + \lambda}, \quad (2.14)$$

and substituting Eq. (2.14) into Eq. (2.13) leads to the so-called structure score that evaluates the quality of a given tree structure [42]:

$$\tilde{\mathcal{L}}_{\text{struct}} = -\frac{1}{2} \sum_{j=1}^{L_t} \frac{G_j^2}{H_j + \lambda} + \gamma L_t. \quad (2.15)$$

When considering a candidate split that divides a leaf I into left and right subsets I_L and I_R , with corresponding gradient sums (G_L, H_L) and (G_R, H_R) , the improvement in the structure score is quantified by the split gain [34]:

$$\text{Gain} = \frac{1}{2} \left[\frac{G_L^2}{H_L + \lambda} + \frac{G_R^2}{H_R + \lambda} - \frac{(G_L + G_R)^2}{H_L + H_R + \lambda} \right] - \gamma. \quad (2.16)$$

This quantity serves as the criterion for determining whether a proposed split is beneficial, and therefore governs the tree-growing process in XGBoost.

2.2 Data input and feature engineering construction

All nuclear properties employed in this study—including proton number, neutron number, α -decay energy Q_α , spin–parity assignments, experimentally measured half-lives $T_{1/2}$, and deformation-related structural parameters—were obtained from the most recent nuclear data evaluations reported in Refs. [24–27, 43]. After consistency verification, these data serve as the basis for constructing the input feature set used in the machine-learning model.

The overall modeling workflow consists of two conceptually independent components addressing distinct physical observables. One component employs an XGBoost-based regression model to predict the α -decay energy Q_α , aiming to capture the nonlinear relationship between nuclear-structure features and decay energy release. The other component independently models the α -decay half-life by incorporating experimentally measured decay energies together with nuclear-structure parameters, enabling a direct investigation of the physical factors governing $T_{1/2}$ without introducing uncertainty propagation from decay-energy prediction.

2.2.1 Decay Energy Prediction

To accurately predict the decay energy, five physically meaningful nuclear features were selected as input parameters for the model, and their definitions are summarized in Table 1.

Name	Relevant Calculations
Mass number	A
Proton number	Z
Neutron number	N
Proton–neutron ratio	Z/N
Relative neutron excess	$(N - Z)/A$

Table 1. Decay energy prediction-related features.

These variables represent fundamental nuclear properties and nucleon configurations within the atomic nucleus. As key determinants of binding energy and decay behavior, they exhibit strong nonlinear correlations with the decay energy—a relationship well supported by both the liquid-drop model and shell-model frameworks [44, 45]. Maintaining a consistent set of input features across light, heavy, and superheavy mass regions enhances the model’s generalizability over the full nuclear chart.

In this study, a total of 1,623 nuclides with positive decay energies ($Q > 0$) were included. Using a 9:1 train–test division, 162 nuclides were randomly selected for independent testing. The model demonstrates strong predictive performance, with detailed numerical results and SHAP-based interpretability analysis presented in the following section.

2.2.2 Half-life Prediction

This stage constitutes the core component of the methodological framework developed in this study. In this part, the α -decay half-life regression model is constructed by incorporating the decay energy Q_α together with multiple nuclear-structure features. All feature parameters employed in the half-life prediction task are summarized in Table 2.

Name	Relevant Calculations
Coefficient of the inverse square root of Q_α	$1/\sqrt{Q_\alpha}$
Decay energy	Q_α
Neutron–proton ratio of the parent nucleus	N_1/Z_1
Neutron number of the parent nucleus	N_1
Minimum angular momentum	ℓ_{\min}
Relative neutron excess of the parent nucleus	$(N_1 - Z_1)/A_1$
Z_1 magic number distance	$ Z_1 - \text{magic} _{\min}$
Mass number of the parent nucleus	A_1
Deformation correction term	$\sqrt{\kappa_2\beta_2}$
Proton number of the parent nucleus	Z_1

Table 2. Feature set used in the half-life prediction model.

In the feature system constructed for this study, the mass number A_1 , neutron number N_1 , and proton number Z_1 of the parent nucleus serve as fundamental structural quantities. These variables determine a nucleus’s position on the nuclear chart and encode essential

information on isospin asymmetry and shell structure, thereby playing an indispensable role in the dynamics of α -decay. Beyond these basic attributes, we further introduce several additional physical quantities related to barrier geometry, energy scales, and quantum selection rules, enabling a more comprehensive description of the mechanisms governing the half-life [46–48].

Among these features, the minimum orbital angular momentum ℓ_{\min} required for α -particle emission constitutes an important descriptor of the centrifugal barrier. Determined by the coupling between the spins (j_p, j_d) and parities (π_p, π_d) of the parent and daughter nuclei, its value follows the selection rules [49]:

$$\ell_{\min} = \begin{cases} \Delta_j, & \text{if } \Delta_j \text{ is even and } \pi_p = \pi_d, \\ \Delta_j + 1, & \text{if } \Delta_j \text{ is even and } \pi_p \neq \pi_d, \\ \Delta_j, & \text{if } \Delta_j \text{ is odd and } \pi_p \neq \pi_d, \\ \Delta_j + 1, & \text{if } \Delta_j \text{ is odd and } \pi_p = \pi_d, \end{cases} \quad \Delta_j = |j_p - j_d|. \quad (2.17)$$

This quantity represents the lowest orbital angular momentum transfer compatible with angular-momentum and parity conservation. Since larger values of ℓ_{\min} raise the effective barrier through the centrifugal term, thereby suppressing tunneling probability and increasing the half-life, its physical influence is well established in α -decay systematics. Although ℓ_{\min} is not among the leading contributors in the SHAP feature ranking, its impact aligns consistently with quantum-tunneling theory and empirical hindrance-factor studies, further validating the physical soundness of our feature-engineering strategy.

The relative neutron excess and the neutron-to-proton ratio are employed to characterize the asymmetry in nucleon distribution within the parent nucleus. These quantities serve as key indicators of nuclear binding and structural stability, as they directly correspond to the symmetry-energy term in the liquid-drop model. Their variations reflect the degree to which a nucleus deviates from the valley of stability. For neutron-rich nuclides far from stability, isospin asymmetry plays a dominant role in shaping the decay barrier and influencing the preformation probability of the α cluster, thereby exerting a significant impact on decay behavior [50, 51]. Incorporating such asymmetry-related parameters into the feature set enables the model to more accurately capture systematic trends across isotopic chains, ultimately improving half-life predictions for exotic and weakly bound nuclei.

To characterize the proximity of the parent nucleus to proton shell closures, we introduce the minimum proton magic-number distance ΔZ_{magic} , which quantifies the influence of shell structure on the α -decay half-life [52–54]. The proton magic numbers considered in this work are 2, 8, 20, 28, 50, 82, and 114. Nuclei located near shell closures generally possess enhanced binding energy and increased structural stability, which significantly affect the shape of the decay barrier and the preformation probability of the α cluster. Thus, this feature effectively strengthens the model’s sensitivity to shell effects.

To further examine the impact of nuclear deformation on the α -decay half-life, a deformation-related correction term $\sqrt{\kappa_2 \beta_2}$ is introduced. Not all nuclei possess perfectly spherical shapes; for the majority of medium and heavy nuclei, spontaneous symmetry

breaking leads to noticeable deformation, which manifests as a pronounced electric quadrupole moment. The nuclear surface is often parametrized by standard deformation variables, among which the quadrupole deformation parameter β_2 is the simplest and most influential, as it governs the dominant deformation effects on the decay barrier [55–60].

To describe the contribution of quadrupole deformation in the daughter nucleus, different values of the coefficient κ_2 are assigned according to the deformation type: $\kappa_2 = 2$ for prolate shapes ($\beta_2 > 0$), $\kappa_2 = -1$ for oblate shapes ($\beta_2 < 0$), and $\kappa_2 = 0$ when the nucleus is nearly spherical ($\beta_2 = 0$). This assignment is designed to embed, within the empirical modeling framework, the qualitative influence of distinct deformation modes on the α -decay half-life.

By combining the deformation sign information (κ_2) with the deformation magnitude (β_2), the constructed term $\sqrt{\kappa_2\beta_2}$ effectively captures the modification of the half-life arising from deformation-induced changes in the Coulomb barrier [43, 61, 62]. Incorporating this feature enhances the model’s sensitivity to barrier-geometry effects and improves its physical consistency across nuclei exhibiting different deformation characteristics.

The selection of these features is grounded in well-established nuclear-physics models, enabling a deeper understanding of nuclear structural stability and the underlying mechanisms governing α -decay. By systematically incorporating key physical effects—such as shell structure, isospin asymmetry, angular-momentum conservation, and nuclear deformation—into the feature space, the model achieves enhanced predictive accuracy and improved physical consistency. This physically informed feature design further strengthens the generalization capability of our half-life framework and provides a more robust basis for interpreting the model’s predictions.

We adopted a 9:1 ratio to partition the dataset into training and test subsets. The detailed predictive performance of the model, together with the SHAP-based interpretability analysis, is presented in Section 3.

2.3 Empirical Formulas (Royer and Universal Decay Law)

In studies of α -decay half-lives, empirical formulas with compact analytical forms are widely employed for rapid estimation owing to their computational efficiency. Such models frequently serve as benchmark references for theoretical frameworks, where nuclide classification schemes are often incorporated to improve predictive performance. Although they do not explicitly describe all microscopic mechanisms, they continue to play a central role in systematics-based investigations of nuclear decay.

In this work, we adopt two of the most widely used and continuously refined empirical formulations: the Royer formula and the Universal Decay Law (UDL). A brief introduction to their analytical structures is provided in this section, and both will be utilized as comparative benchmarks in subsequent analyses to evaluate the physical consistency and predictive capability of our machine-learning framework.

2.3.1 Royer Formula

The Royer formula, originally proposed by G. Royer, is derived from the liquid-drop model and subsequently fitted to extensive experimental datasets [7–9, 27]. This empirical ex-

pression is applicable to nuclides with different proton–neutron parity combinations, and its general form is given by:

$$\log_{10} T_{1/2}^{\text{Royer}} = a + bA^{1/6}\sqrt{Z} + \frac{cZ}{\sqrt{Q_\alpha}}, \quad (2.18)$$

to extend the applicability of the Royer expression to α -decay processes involving non-zero angular momentum transfer, G. Royer and collaborators introduced an angular-momentum correction term. Furthermore, to account for the influence of nuclear deformation on the half-life, we incorporate an additional quadrupole deformation term of the daughter nucleus into the formulation. Accordingly, in this study we adopt the modified Royer expression presented in Refs. [12, 27, 59, 60, 62] as the empirical benchmark for comparison.

$$\log_{10} T_{1/2}^{\text{Royer}} = a + bA^{1/6}\sqrt{Z} + \frac{cZ}{\sqrt{Q_\alpha}} + \frac{\ell(\ell+1)}{\sqrt{(A-4)(Z-2)}A^{2/3}} + d\sqrt{\kappa_2\beta_2} \frac{Z}{\sqrt{Q_\alpha}}, \quad (2.19)$$

Here, A denotes the mass number of the parent nucleus, Z is the proton number, and Q_α represents the decay energy. The determination of κ_2 follows exactly the same convention described earlier, and the same rule also applies to the UDL formulation. The coefficients a , b , c , and d are fitted parameters whose values depend on the even–odd structure of the parent nucleus. The corresponding parameter sets for the four nucleon-parity classifications (e–e, e–o, o–e, and o–o) are summarized in Table 3.

Nuclei	a	b	c	d
e–e	-25.3100	-1.1629	1.5864	-0.0106
e–o	-26.6500	-1.0859	1.5848	-0.0186
o–e	-25.6800	-1.1423	1.5920	0.0156
o–o	-20.4800	-1.1130	1.6971	-0.0223

Table 3. Coefficients in the Royer formula.

2.3.2 Universal Decay Law Formula

The UDL formula offers several significant advantages. Unlike purely empirical expressions, it is derived from a clear physical foundation that encapsulates the essential mechanism of barrier penetration in radioactive decay. Moreover, the UDL provides a unified description for both α decay and heavier cluster radioactivities, enabling consistent application across different decay modes within a single theoretical framework. It also exhibits strong predictive performance for even–even, odd–even, and odd–odd nuclei, and can be reliably extrapolated to the superheavy region, offering valuable insights into the structural stability of newly synthesized elements [10, 62, 63].

$$\log_{10} T_{1/2}^{\text{UDL}} = a \frac{\sqrt{\mu} Z_\alpha Z_d}{\sqrt{Q_\alpha}} + b \left[\sqrt{\mu} Z_\alpha Z_d \left(A_\alpha^{1/3} + A_d^{1/3} \right) \right]^{1/2} + c + d\ell(\ell+1) + eI + fI^2. \quad (2.20)$$

Similarly, by incorporating the quadrupole deformation parameter β_2 into the original UDL formulation, nuclear shape effects can be further embedded within the empirical

description. This modification enables a more comprehensive representation of deformation-induced changes in the decay barrier and consequently the half-life. The resulting expression takes the following form [27, 59, 60, 62]:

$$\log_{10} T_{1/2}^{\text{UDL}} = a\sqrt{\mu Z_\alpha Z_d} \frac{1}{\sqrt{Q_\alpha}} + b \left[\sqrt{\mu Z_\alpha Z_d} \left(A_\alpha^{1/3} + A_d^{1/3} \right) \right]^{1/2} + c + d\ell(\ell + 1) + eI + fI^2 + g\sqrt{\kappa_2\beta_2} \frac{Z}{\sqrt{Q_\alpha}}. \quad (2.21)$$

Among the terms appearing in the UDL expression, $Z_\alpha = 2$ and $A_\alpha = 4$ denote the proton number and mass number of the emitted α particle, respectively. The fitting coefficients of the UDL formula depend on the even–odd parity combination of the parent nucleus’s proton and neutron numbers, corresponding to four distinct cases summarized in Table 4.

Both empirical formulations—the Royer model and the UDL—have undergone extensive validation in α -decay systematics. Although they cannot fully reproduce all microscopic mechanisms, they provide essential phenomenological frameworks for understanding global decay trends. Building upon these foundations, we subsequently generate half-life predictions using both empirical models and perform a comprehensive comparative analysis against the results obtained from our machine learning framework.

Nuclei	a	b	c	d	e	f	g
e–e	0.4226	-0.5582	-25.116	0	2.5165	-27.929	-0.0183
e–o	0.4290	-0.5504	-25.916	0.04578	-15.408	43.457	-0.0218
o–e	0.4275	-0.5428	-24.855	0.0135	-16.031	32.542	-0.0085
o–o	0.4341	-0.5424	-26.0589	0.0401	-6.7131	14.46	-0.0235

Table 4. Coefficients used in the empirical α -decay half-life formula for different odd–even combinations of parent nuclei.

3 Results and Discussion

3.1 Decay Energy Prediction Performance

To quantitatively evaluate the predictive performance of the decay-energy model, we summarize the key error metrics for both the training and test sets. As shown in Table 5, the model achieves consistently high accuracy with only minor discrepancies between the two sets. This indicates excellent generalization capability and confirms that no significant overfitting is present.

Type	RMSE	MAE
Training Set	0.2482	0.1229
Test Set	0.2562	0.1726

Table 5. Performance metrics for training and test sets.

The model achieves extremely high fitting accuracy on the training set while maintaining strong predictive performance on the test set, demonstrating excellent generalization

capability. Although the prediction error on the test set is slightly larger than that on the training set, it remains at a low level overall, indicating that the model effectively handles previously unseen nuclides and provides reliable support for the analysis of decay-energy systematics and subsequent result discussions.

Having obtained stable and physically consistent decay-energy predictions, it is essential to further investigate the physical factors the model relies on during learning. To this end, we employed the SHAP framework to conduct a feature importance analysis, enabling a quantitative assessment of the contributions made by various nuclear-structure features to the prediction output. The interpretability results are presented in Fig. 1.

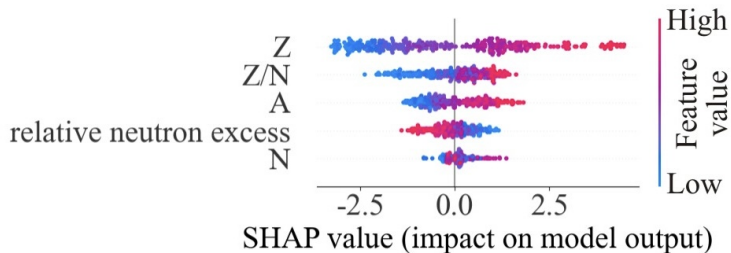


Figure 1. SHAP summary plot showing the feature importance distribution in the decay energy prediction model. The horizontal axis represents SHAP values, indicating the impact of each feature on the model output per sample. Each dot corresponds to a single prediction instance, colored according to the feature value from low (blue) to high (red).

Figure 1 presents the SHAP feature importance distribution for decay-energy prediction. The model primarily relies on proton number Z , neutron number N , mass number A , and symmetry-energy-related quantities such as Z/N and the relative neutron excess. The importance ranking of these features is consistent with liquid-drop and shell-model expectations, indicating that the model successfully captures the known systematic behavior of nuclear binding energies.

Overall, the essential nuclear-structure information relevant to Q_α is effectively captured, demonstrating the model’s ability to learn physically meaningful correlations within the decay-energy systematics.

3.2 Half-Life Prediction Performance

To quantify the baseline performance of traditional analytical approaches, we evaluate the Royer and UDL formulas on the full α -decay dataset used in this work. Their global prediction errors, summarized in Table 6, represent the characteristic accuracy achievable by empirical relations. As expected, the UDL formula exhibits substantially better overall performance than the Royer expression, reflecting its more complete incorporation of decay-systematics trends. These baseline values provide a quantitative reference for subsequent comparison with the machine-learning model presented later in this section.

Model	RMSE	MAE
UDL Formula	0.8887	0.6839
Royer Formula	3.0897	1.4727

Table 6. Overall prediction errors of the Royer and UDL formulas on the full α -decay dataset.

For the half-life prediction, an α -decay half-life regression model is constructed by combining decay-energy information with multiple nuclear-structure features. To quantitatively and systematically evaluate the predictive performance of the model, three core metrics— R^2 , RMSE, and MAE—are calculated for both the training and test sets. The results indicate that the model achieves near-optimal fitting accuracy on the training set while maintaining a high level of predictive performance on the test set. Although the errors on the test set are slightly larger than those on the training set, they remain within a low and acceptable range, with no evident signs of overfitting. Overall, the model demonstrates robust generalization capability across previously unseen nuclides, thereby providing a reliable basis for subsequent physical analysis and comparison with empirical formulas. The corresponding evaluation metrics are summarized in Table 7.

Type	RMSE	MAE
Training Set	0.5031	0.3422
Test Set	0.5192	0.3907

Table 7. Performance metrics for the α -decay half-life prediction model.

After establishing the superior predictive accuracy of the XGBoost-based half-life regression model compared with the Royer and UDL empirical formulas—supported by both quantitative performance metrics (Table 7) and model–data comparison plots (Fig. 2)—it becomes necessary to further examine the physical origin of this improvement. In particular, a deeper understanding is required of how the model utilizes multidimensional nuclear-structure inputs and how each physical feature contributes to the predicted decay half-lives.

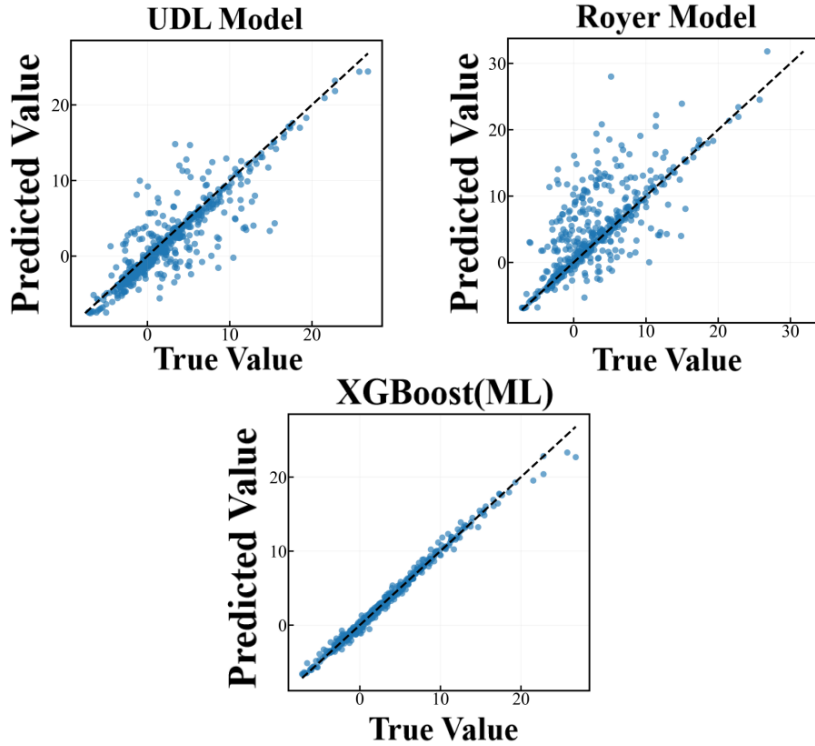


Figure 2. Scatter plots comparing the predicted and experimental values of $\log_{10}(T_{1/2})$ using the XGBoost model, the Royer empirical formula, and the UDL formula. Each panel shows the correlation between model predictions and experimental data, with the dashed line representing the ideal prediction curve.

Since α -decay half-lives are simultaneously influenced by decay energy, centrifugal-barrier effects, shell structure, nuclear deformation, and isospin asymmetry, interpreting the internal decision process of the machine-learning model is essential for validating its physical consistency. To this end, we employ the SHAP (SHapley Additive exPlanations) interpretability framework to analyze the trained XGBoost model. SHAP enables a quantitative decomposition of the prediction into contributions from individual physical features and allows verification of whether the learned dependencies follow established nuclear-structure and decay systematics.

The resulting feature-importance distribution is displayed in Fig. 3.

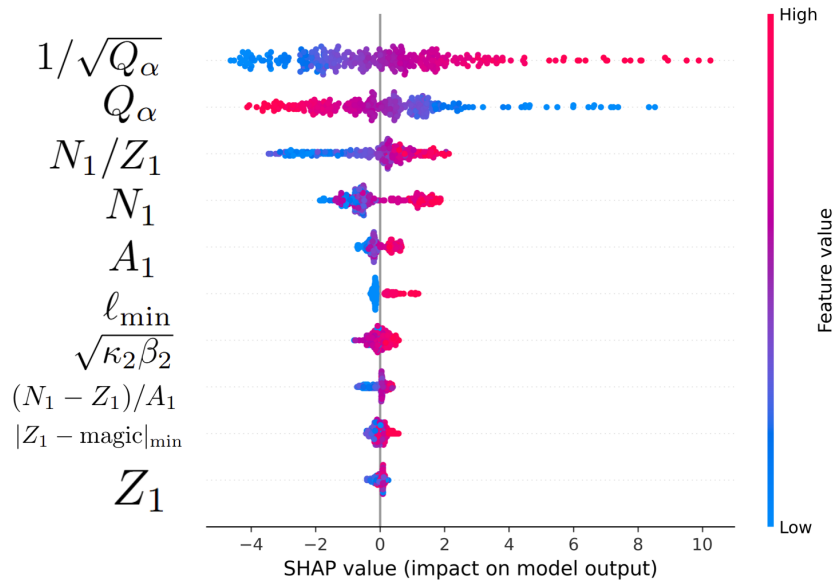


Figure 3. SHAP-based feature importance for the α -decay half-life prediction model.

Figure 3 presents the SHAP feature-importance distribution for the half-life regression model. A clear hierarchical structure of physical contributions emerges. The dominant influence arises from $1/\sqrt{Q_\alpha}$ and Q_α , whose SHAP amplitudes are substantially larger than those of all other features. Large values of $1/\sqrt{Q_\alpha}$ (corresponding to low decay energies) predominantly yield positive SHAP contributions, increasing $\log_{10} T_{1/2}$, whereas higher Q_α values produce negative SHAP contributions and shorten the predicted half-life. This trend is fully consistent with the WKB barrier-penetration picture and the Geiger–Nuttall law, demonstrating that the model internalizes the exponential sensitivity of α decay to the decay energy.

Subleading contributions originate from N_1/Z_1 , N_1 , and A_1 , reflecting the roles of nucleon-number systematics, isospin asymmetry, and the overall mass scale. Their SHAP distributions exhibit stable, monotonic patterns, indicating that the model captures symmetry-energy effects, shell-structure corrections, and the characteristic behavior of neutron-rich nuclei rather than relying solely on energy variables.

The minimum orbital angular momentum ℓ_{\min} constitutes one of the most physically interpretable features in the model. Larger values of ℓ_{\min} , associated with a higher centrifugal barrier, systematically produce positive SHAP contributions and extend the predicted half-life, in agreement with the well-known angular-momentum hindrance mechanism. The deformation-related term $\sqrt{\kappa_2\beta_2}$ provides a moderate but non-negligible contribution, with SHAP values that vary according to the sign and magnitude of β_2 . This behavior reflects the modification of the Coulomb barrier due to nuclear deformation.

Additional features such as the proton number Z_1 and the distance to the nearest magic number contribute at a secondary yet physically meaningful level. Their nonzero SHAP amplitudes indicate that the model incorporates shell effects to refine predictions in regions

where empirical formulas typically experience systematic deviations.

Overall, the SHAP analysis confirms that the XGBoost regression model does not operate as a black-box interpolator. Instead, it reproduces the established hierarchical dependence of α -decay half-lives on decay energy, isospin asymmetry, angular momentum, deformation, and shell structure. This physically interpretable learning behavior explains the model’s systematic improvement over empirical formulas while remaining consistent with known nuclear decay systematics.

4 Summary and Conclusion

In this work, we have developed a physics-informed machine-learning framework to systematically investigate α -decay energies and half-lives across a broad range of nuclides. The framework is constructed on the eXtreme Gradient Boosting (XGBoost) regression algorithm and incorporates physically motivated nuclear-structure descriptors, including mass and charge numbers, isospin asymmetry, shell proximity, minimum orbital angular momentum transfer, and quadrupole deformation. By embedding established physical considerations into a data-driven modeling strategy, the proposed approach achieves high predictive accuracy while maintaining strong generalization capability.

For the α -decay energy prediction, the XGBoost model demonstrates excellent agreement with evaluated experimental data over the full dataset. The corresponding SHAP-based analysis confirms that the dominant feature contributions follow well-established decay-energy systematics, indicating that the model captures physically meaningful correlations rather than relying on purely numerical fitting. These results suggest that the proposed framework provides a reliable and interpretable description of α -decay energy trends.

Independently, an α -decay half-life regression model is constructed by combining experimentally measured decay energies with multiple nuclear-structure features. The model exhibits near-optimal fitting performance on the training set and maintains a high level of predictive accuracy on independent test nuclides, with no evident signs of overfitting. When benchmarked against widely used empirical formulations, including the Royer and Universal Decay Law (UDL) expressions, the machine-learning approach yields lower overall prediction errors while preserving the established physical trends captured by traditional models. This demonstrates that the proposed framework can be viewed as a natural extension of empirical systematics, offering enhanced quantitative precision without compromising physical consistency.

Furthermore, SHAP-based interpretability analysis provides additional insight into the internal decision mechanisms of the half-life model. The dominant roles of decay energy, angular-momentum hindrance, shell effects, and nuclear deformation are found to be consistent with theoretical expectations derived from quantum tunneling descriptions of α decay. This agreement supports the reliability and physical transparency of the learned feature–target relationships across diverse nuclear regions.

Overall, the present study illustrates that physics-guided gradient-boosting models can serve as accurate, robust, and interpretable tools for nuclear decay modeling. Future work

may incorporate microscopic preformation factors, enrich deformation-related inputs, and extend the present framework to other decay modes such as cluster radioactivity and proton emission. In addition, the approach may be applied to the prediction and interpretation of decay properties in regions where experimental data remain scarce, including yet-unobserved superheavy nuclei.

5 Acknowledgements

This work is supported by Yunnan Provincial Science Foundation Project (No. 202501AT070067), Yunnan Provincial Xing Dian Talent Support Program (Young Talents Special Program, (Young Talents Special Program, No. XDYC-QNRC-2023-0162), Kunming University Talent Introduction Research Project (No. YJL24019), Yunnan Provincial Department of Education Scientific Research Fund Project (No. 2025Y1055 and 2025Y1042), the Program for Frontier Research Team of Kunming University 2023, National Natural Science Foundation of China (No. 12063006), National College Student Innovation and Entrepreneurship Training Program (No. 202511393012, 202511393013, and 202511393016) , and Yunnan Province College Student Innovation and Entrepreneurship Training Program (No. S202511393003, S202511393043, and S202511393044).

References

- [1] Rutherford E and Royds T 1909 *The London, Edinburgh, and Dublin Philosophical Magazine and Journal of Science* **17** 281–286
- [2] Rutherford E 1899 *The London, Edinburgh, and Dublin Philosophical Magazine and Journal of Science* **47** 109–163
- [3] Rutherford E and Geiger H 1908 *Proceedings of the Royal Society of London. Series A, Containing Papers of a Mathematical and Physical Character* **81** 141–161
- [4] Geiger H and Nuttall J 1911 *The London, Edinburgh, and Dublin Philosophical Magazine and Journal of Science* **22** 613–621
- [5] Gamow G 1928 *Zeitschrift für Physik* **51** 204–212
- [6] Gurney R W and Condon E U 1928 *Nature* **122** 439–439
- [7] Royer G 2000 *Journal of Physics G: Nuclear and Particle Physics* **26** 1149
- [8] Deng J G, Zhang H F and Royer G 2020 *Physical Review C* **101** 034307
- [9] Dong J, Zhang H, Wang Y, Zuo W and Li J 2010 *Nuclear Physics A* **832** 198–208
- [10] Qi C, Liotta R J and Wyss R 2021 *Physics Letters B* **818** 136373
- [11] Kelkar N and Nowakowski M 2014 *Physical Review C* **89** 014602
- [12] Wang Y, Dong J, Peng B and Zhang H 2010 *Physical Review C—Nuclear Physics* **81** 067301
- [13] Liu X, Jiang J D, Wu X J and Li X H 2024 *Chinese Physics C* **48** 054101
- [14] Mumpower M R, Sprouse T M, Lovell A E and Mohan A T 2022 *Physical Review C* **106** L021301

- [15] He W, Li Q, Ma Y, Niu Z, Pei J and Zhang Y 2023 *Science China Physics, Mechanics & Astronomy* **66** 282001
- [16] Shinde P P and Shah S 2018 A review of machine learning and deep learning applications *2018 Fourth international conference on computing communication control and automation (ICCUBEA)* (IEEE) pp 1–6
- [17] LeCun Y, Bengio Y and Hinton G 2015 *nature* **521** 436–444
- [18] Zhang J M, Harman M, Ma L and Liu Y 2020 *IEEE Transactions on Software Engineering* **48** 1–36
- [19] Jin Z, Yan M, Zhou H, Cheng A, Ren Z and Liu J 2023 *Physical Review C* **108** 014326
- [20] Ma N N, Zhao T L, Wang W X and Zhang H F 2023 *Physical Review C* **107** 014310
- [21] Saxena G, Jain A and Sharma P 2021 *Physica Scripta* **96** 125304
- [22] You H Q, Qu Z Z, Wu R H, Su H Z and He X T 2022 *Symmetry* **14** 1006
- [23] Li C Q, Tong C N, Du H J and Pang L G 2022 *Physical Review C* **105** 064306
- [24] Kondev F, Wang M, Huang W, Naimi S and Audi G 2021 *Chinese Physics C* **45** 030001
- [25] Huang W, Wang M, Kondev F G, Audi G and Naimi S 2021 *Chinese Physics C* **45** 030002
- [26] Wang M, Huang W J, Kondev F G, Audi G and Naimi S 2021 *Chinese Physics C* **45** 030003
- [27] Möller P, Sierk A J, Ichikawa T and Sagawa H 2016 *Atomic Data and Nuclear Data Tables* **109** 1–204
- [28] Cai B, Chen G, Xu J, Yuan C, Qi C and Yao Y 2020 *Physical Review C* **101** 054304
- [29] Hosseini-Tabatabaei M, Alavi S and Dehghani V 2021 *Canadian Journal of Physics* **99** 24–32
- [30] Zhang H and Royer G 2008 *Physical Review C—Nuclear Physics* **77** 054318
- [31] Denisov V Y and Khudenko A 2009 *Physical Review C—Nuclear Physics* **79** 054614
- [32] Ahsan M M, Mahmud M P, Saha P K, Gupta K D and Siddique Z 2021 *Technologies* **9** 52
- [33] De Amorim L B, Cavalcanti G D and Cruz R M 2023 *Applied Soft Computing* **133** 109924
- [34] Chen T 2016 *Cornell University*
- [35] Li Y, Feng Y and Qian Q 2023 *Journal of Information Security and Applications* **74** 103468
- [36] Shree S M and Balasubramaniam M 2025 *The European Physical Journal A* **61** 32
- [37] Zhang Y and Chen L 2021 *Theoretical economics letters* **11** 258–267
- [38] Zühlke M M and Kudenko D 2025 *Machine Learning* **114** 108
- [39] Zhou Z H 2025 *Ensemble methods: foundations and algorithms* (CRC press)
- [40] Friedman J H 2001 *Annals of statistics* 1189–1232
- [41] Sluijterman L, Kreuwel F, Cator E and Heskes T 2025 *International Journal of Machine Learning and Cybernetics* 1–15
- [42] Dong X, Lei T, Jin S and Hou Z 2018 Short-term traffic flow prediction based on xgboost *2018 IEEE 7th data driven control and learning systems conference (DDCLS)* (IEEE) pp 854–859
- [43] Denisov V Y 2025 *Atomic Data and Nuclear Data Tables* **161** 101684

- [44] Royer G 2008 *Nuclear Physics A* **807** 105–118
- [45] Zhang H, Zuo W, Li J and Royer G 2006 *Physical Review C—Nuclear Physics* **74** 017304
- [46] Seif W and Adel A 2019 *Physical Review C* **99** 044311
- [47] Sheline R K and Bossinga B B M 1991 *Physical Review C* **44** 218
- [48] Delion D, Liotta R and Wyss R 2007 *Physical Review C—Nuclear Physics* **76** 044301
- [49] Saxena G, Sharma P and Saxena P 2021 *Journal of Physics G: Nuclear and Particle Physics* **48** 055103
- [50] Cui J, Gao Y, Wang Y and Gu J 2022 *Nuclear Physics A* **1017** 122341
- [51] Otsuka T, Gade A, Sorlin O, Suzuki T and Utsuno Y 2020 *Reviews of modern physics* **92** 015002
- [52] Nakada H 2019 *Physical Review C* **100** 044310
- [53] Sorlin O and Porquet M G 2008 *Progress in Particle and Nuclear Physics* **61** 602–673
- [54] Amiel S and Feldstein H 1975 *Physical Review C* **11** 845
- [55] Stone N 2016 *Atomic Data and Nuclear Data Tables* **111** 1–28
- [56] Ma L, Wang K, Xie Y, Yang X, Wang Y, Zhou M, Liu H, Yu X, Zhao Y, Wang H *et al.* 2022 *Physical Review Letters* **128** 167001
- [57] Butler P 2023 Studies of heavy pear-shaped nuclei *Journal of Physics: Conference Series* vol 2453 (IOP Publishing) p 012001
- [58] Garrett P E, Zielińska M and Clément E 2022 *Progress in Particle and Nuclear Physics* **124** 103931
- [59] Qian Y and Ren Z 2012 *Journal of Physics G: Nuclear and Particle Physics* **39** 115106
- [60] Manhas M and Gupta R K 2005 *Physical Review C—Nuclear Physics* **72** 024606
- [61] Denisov V Y 2024 *Physical Review C* **110** 014604
- [62] Yazdankish E and Nejatollahi M 2023 *Physica Scripta* **98** 115309
- [63] Zhao T and Zhang H 2022 *Journal of Physics G: Nuclear and Particle Physics* **49** 105104